Two resting potential levels regulated by the inward-rectifier potassium channel in the guinea-pig spiral modiolar artery

Zhi-Gen Jiang*, Jun-Qiang Si*†, Michael R. Lasarev‡ and Alfred L. Nuttall*§

**Oregon Hearing Research Center and ‡Center for Research on Occupational and Environmental Toxicology, Oregon Health and Science University, Portland, OR 97201, USA, † Department of Physiology, Shihezi University Medical College, Xinjiang, People's Republic of China and § Kresge Hearing Research Institute, University of Michigan, Ann Arbor, MI 48109, USA*

(Resubmitted 7 June 2001; accepted after revision 23 August 2001)

1. Intracellular *in vitro* recordings were made from 771 cells from the spiral modiolar artery (SMA). The initial resting potentials (RPs) displayed a bimodal distribution that was well modelled as a mixture of two Gaussian distributions. About half of the cells had an average RP of −74 mV, and were termed high-RP cells, whereas the other half had an average RP around −41 mV, and were termed low-RP cells. Preparations that were incubated for longer than 24 h contained significantly more high-RP cells than those incubated for less than 8 h.

2. When labelled with the fluorescent dye propidium iodide, 68 and 36 cells were identified as smooth muscle cells (SMC) and endothelial cells (EC), respectively. The RP and input resistance were not significantly different between these two types of cell. Dye coupling was observed only in ECs. Dual cell recordings with 0.2–1.0 mm separation demonstrated the simultaneous existence of high- and low-RP cells and a heterogeneous low-strength electrical coupling.

3. The high-RP cells were depolarized by ACh and by high extracellular potassium concentration (high K^+). The low-RP cells were usually hyperpolarized by moderately high K^+ (7.5–20 mM) and by ACh. The high K^+-induced hyperpolarization was suppressed by barium (Ba^{2+}, 10–50 μM). The putative gap junction blocker 18β-glycyrrhetinic acid suppressed the ACh-induced responses in SMCs, but not in ECs.

4. Low-RP cells could rapidly shift the membrane potential to a permanent high-RP state spontaneously or, more often, after a brief application of hyperpolarizing agents including high K^+, ACh, nitric oxide and pinacidil. Once shifted to a high-RP state, the responses of these cells to high K^+ and ACh became similar to those of the original high-RP cells.

5. High-RP cells occasionally shifted their potentials to a low-RP state either spontaneously or after a brief application of 10–50 μM Ba^{2+} or 100 μM ouabain. Once shifted to the low-RP state, the response of these cells to high K^+ and ACh became a hyperpolarization. The shift between high- and low-RP states was largely mimicked by wash-in and wash-out of low concentrations of Ba^{2+}. The shift often showed a regenerative process as a fast phase in its middle course.

6. It is concluded that the cochlear SMA *in vitro* is composed of poorly and heterogeneously coupled SMCs and ECs, simultaneously resting in one of two distinct states, one a high-RP state and the other a low-RP state. The two RP states are exchangeable mainly due to all-or-none-like conductance changes of the inward-rectifier K^+ channel.

The membrane potential of vascular smooth muscle cells (SMCs) is a major determinant of cytosolic free Ca^{2+} concentrations, and thus the myogenic tone (Nelson *et al.* 1990; Faraci & Sobey, 1998). In small arteries, vascular tone may just be related to the degree of depolarization, without the involvement of action potentials (Nelson *et al.* 1990; Knot & Nelson, 1998). The resting potential (RP) level varies a great deal among reports using different vessel preparations and recording methods. Microelectrode measurements in unpressurized *in vitro* small arteries and arterioles under baseline conditions generally have a RP range from −60 to −75 mV (Hirst & Edwards, 1989; Nelson *et al.* 1990; Faraci & Sobey, 1998). In distal segments of the cerebral arterioles (Edwards *et al.* 1988), arteries

pressurized to about 60 mmHg (Dietrich & Dacey, 1994; Knot & Nelson, 1995), and arteries in *in vivo* conditions (Welsh & Segal, 1998), the RP of the SMC is about −40 mV.

Potassium (K^+) channels, like in most other excitable and non-excitable cells, constitute a major part of the resting membrane conductance in the vascular SMCs and endothelial cells (ECs). The main K^+ channel types, including voltage-dependent delayed-rectifier (K_{DR}), calcium-activated (K_{Ca}), A-like (K_A), inward-rectifier (K_{ir}) and ATP-sensitive (K_{ATP}) K^+ channels, have all been identified in blood vessel SMCs (Nelson *et al.* 1990; Quayle *et al.* 1997; Faraci & Sobey, 1998) and some in ECs (Chen & Cheung, 1992; Zhang *et al.* 1994; Suvatne *et al.* 2001). However, their expression levels and functional roles vary significantly among the vessel beds. For example, it is reported that K_{ir} is a dominating resting conductance that makes a major contribution to setting the RP in some submucosal, coronary and cerebral arteries (Edwards & Hirst, 1988; Edwards *et al.* 1988; Quayle *et al.* 1993; Knot *et al.* 1996). On the other hand, K_{ir} has been found to play little or no role in setting of the RP in the rabbit renal arcuate artery (Prior *et al.* 1998), pulmonary artery (Bae *et al.* 1999) and most big arteries (Quayle *et al.* 1997).

Circulation disturbances have been implicated in hearing losses caused by loud sound, ageing, Meniere's disease, some forms of sudden deafness (Hultcrantz, 1988; Schuknecht & Gacek, 1993; Suzuki *et al.* 1998) and in increased sensitivity to ototoxic drugs and noise-induced trauma (Kimura, 1986). Little work has been done regarding the physiology of the inner ear vasculature, particularly at the cellular and subcellular levels. The cochlear spiral modiolar artery (SMA) conducts the major blood supply of the cochlea. Using an isolated guinea-pig SMA preparation and conventional intracellular recording methods, over the last few years we have begun to explore the cellular electrophysiology of the vasculature (Jiang *et al.* 1999). The guinea-pig SMA has a diameter of 20–80 μm and one to two layers of SMCs, which are densely innervated by catecholamine-containing fibres. The majority of the vascular cells have a barium (Ba^{2+})-sensitive RP near −80 mV and an input resistance of ∼8 MΩ, suggesting the presence of K_{ir} and an electrical coupling between the cells. Here, we report further that both the SMCs and ECs in the *in vitro* SMA rest at two distinct but exchangeable levels of membrane potential due to all-or-non-like activation of K_{ir}. Preliminary results from these studies have appeared in two meeting abstracts (Jiang & Nuttall, 2000*a*,*b*).

METHODS

Animals and SMA preparation

Guinea-pigs (300–500 g) were killed by exsanguination under general anaesthesia. The anaesthesia was accomplished by I.M. injection of an anaesthetic mixture (1 ml kg^{-1}) of ketamine (500 mg), xylazine (20 mg) and acepromazine (10 mg) in 8.5 ml water. Both bullae were rapidly removed and transferred to a Petri dish filled with a physiological solution (Krebs) composed of (mM): NaCl 125, KCl 5, $CaCl_2$ 1.6, $MgCl_2$ 1.2, NaH_2PO_4 1.2, $NaHCO_3$ 18 and glucose 8.2, and saturated with 95% O_2 and 5% CO_2 at 35°C (pH 7.4). The SMA and some associated radiating arterioles were dissected from the cochlea and incubated for 0.5 h (1st day preparation) or 24 h (2nd day preparation) in the physiological solution, and then transferred to a recording bath chamber for electrophysiological experiments over the next 6–8 h. A segment of the SMA was further dissected free of spongy connective tissues, pinned with minimum stretch to the silicon rubber layer (Sylgard 184, Dow Corning, USA) in the bottom of an organ bath (volume 0.5 ml), and superfused continuously with Krebs solution at 35°C. When needed, high K^+ (10–50 mM) Krebs solution was made with additional KCl and accordingly reduced NaCl. The animal use procedures were approved by the Oregon Health and Science University Animal Care Committee.

Intracellular recording and statistics

Intracellular recordings were made from the proximal SMA of the cochlear base turn to the second turn. Vessel segments were about 5 mm long and 50–80 μm in outside diameter. Microelectrodes were filled with 2 M KCl and had a tip resistance of 50–120 MΩ. Intracellular penetration was obtained by blindly advancing the glass electrode into the adventitial surface of the vessel with the aid of a micromanipulator (MP-1 Narishige, Japan). Transmembrane potential and current were monitored simultaneously by an Axoclamp-2B preamplifier (Axon Instruments, USA). Electrical signals were recorded on a pen recorder (0–60 Hz) and/or a PC computer equipped with Axoscope 8 and pCLAMP 6 software (Axon Instruments) using sampling intervals of 0.1, 0.5 or 10 ms.

Intracellular current injection was carried out via the recording electrode by using the preamplifier, on which the bridge circuit was carefully balanced. The criteria used to identify a successful intracellular penetration were: (1) advancing the electrode caused a sudden jump of the voltage trace from zero to a negative value of no less than −30 mV, with the latter lasting no less than 5 min, (2) application of a high K^+ (10 mM) solution caused a reversible depolarization or hyperpolarization (Figs 3 and 4), and (3) dislocation or withdrawal of the electrode caused a voltage jump back to near zero. The RP was determined by the initial and/or the end voltage jump. The input resistance was estimated by measuring the steady-state membrane potential induced by a 0.2–0.5 nA, 500–1000 ms hyperpolarizing current pulse (Fig. 7*A* and *B*). An average of 5–10 sweeps was often used to improve the signal-to-noise ratio.

The RP data were modelled as a mixture of two Gaussian distributions with parameters estimated through maximum likelihood (Everitt & Hand, 1981; Fig. 2). Likelihood ratio tests were used to compare model parameters across different sets of data (Casella & Berger, 1990). These statistical computations were performed using O-Matrix 4.0 (Harmonic Software). Statistical values are expressed as means ± S.E.M.

Identification of SMCs *vs.* ECs

Some of the intracellularly recorded cells were dye-labelled with a method reported previously (Emerson & Segal, 2001) to identify the cell types. Briefly, the sharp electrodes were tip-filled with the fluorescent dye propidium iodide (1% in 2 M KCl) and back-filled with 2 M KCl. After a stable RP recording for 3–5 min, depolarizing pulses (0.5 nA, 20 ms, 16 Hz for 2 min) were applied to facilitate the dye diffusion. The SMA preparation was mounted in Vectashield (Vector Laboratories) with a coverslip for fluorescence microscope examination (Zeiss, Axiovert 35 equipped with a digital camera, and Metamorph software on a PC computer). The specimen was viewed and photographed in fluorescence mode to visualize the stained nucleus (Fig. 1*A* and *C*) or in combination with the phase-contrast mode for a simultaneous vessel image (Fig. 1*B* and *D*).

Drugs and application

Drugs at known concentrations were applied to the bathing solution. The solution that passed through the recording chamber could be switched, without a change in flow rate or temperature, to one that contained a drug or one of different ionic composition. The drugs used in this study were: ACh, atropine, pinacidil, 8-bromo-cAMP, cAMP Rp-isomer (Rp-cAMPS), charybdotoxin, apamin, L-NAME, 4-aminopyridine (4AP), 18β-glycyrrhetinic acid (18βGRA), ouabain, glipizide (all from Sigma-Research Biochemicals), and DPTA-NONOate (Alexis, USA).

RESULTS

General observations and identification of the cell types

Stable intracellular recordings were made successfully in more than 700 cells randomly penetrated along the segments of the proximal half of 285 SMAs from either side. The recordings lasted from 5 min to 6.5 h.

With the electrode pipette solution containing the fluorescent dye propidium iodide, of the 104 cells examined after electrical recording, 68 were identified as SMCs and 36 as ECs (Fig. 1). The nuclei of recorded cells regularly show strong orange–red fluorescence. The type of the recorded cell could be distinguished unambiguously by the following features (Emerson & Segal, 2001). The nuclei of SMCs were rod shaped and oriented circumferentially to the vessel (Fig. 1*A* and *B*). Multiple SMC staining (dye coupling) after a single SMC penetration was rare ($n = 2$). On the other hand, one or more additional nuclei of ECs were often less intensely stained after a single EC penetration (19 out of 36, Fig. 1*B* and *D*). The EC nuclei were mostly fusiform or rod shaped. The ECs were consistently oriented parallel to the vascular axis. Dye coupling between the SMCs and ECs was never observed. The electrical membrane properties of the SMCs and the ECs were generally not distinguishable from each other (see below and Fig. 2). We henceforth pool them together unless specified otherwise.

Two sets of normal distribution of initial RPs

The initial RP of the recorded cells in the SMA was measured in a normal Krebs solution (5 mM K^+) 5–10 min after cell penetration and membrane potential stabilization. The 5 mV bin histogram of the initial RP levels of 771 cells exhibits a bimodal distribution with a trough between −55 and −64 mV (Fig. 2*A*). The RP data were modelled as a mixture of two Gaussian distributions through maximum likelihood (curve in Fig. 2*A*; Everitt & Hand, 1981). The correlation between the observed

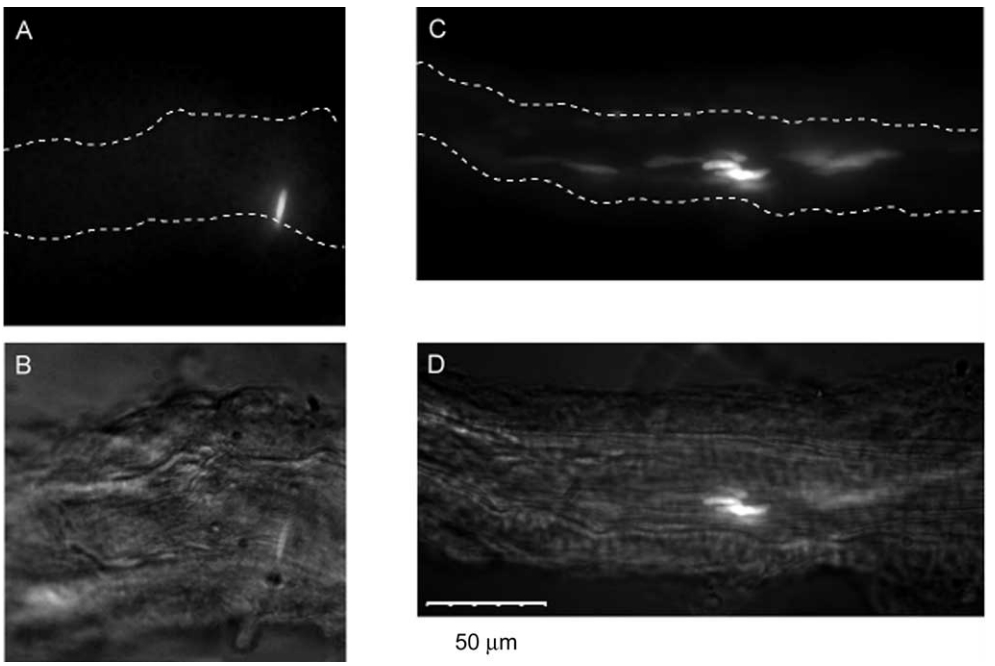

Figure 1. Intracellular labelling of smooth muscle cells and endothelial cells

Cells were impaled with electrodes containing propidium iodide (1 % in 2 M KCl). The dye-stained nuclei, emitting orange–red fluorescence, are shown as bright short rods in the monochrome micrographs. *A* and *C* are examples of a smooth muscle cell (SMC; resting potential, RP −74 mV) recorded for 7 min, and an endothelial cell (EC; RP −69 mV) recorded for 22 min, respectively. The SMCs usually exhibited single cell staining. Their nuclei had an orientation circumferential to the vessel axis, whereas the ECs often showed multiple cell staining with nuclei always parallel to the axis of the spiral modiolar artery (SMA). *B* and *D* are duplicate micrographs of *A* and *C*, respectively, but taken with simultaneous phase-contrast illumination, revealing the contour of the vessels. The lumens (dashed lines) in *A* and *C* were drawn along the lamina propria seen in *B* and *D*.

measurements and those predicted from the mixture model is exceptionally high ($r = 0.998$). The population that peaked at a high negative value had a mean RP of -74 ± 0.46 mV, while the second population had a mean RP of -41 ± 0.52 mV. Cells belonging to the first theoretical Gaussian population (mean at -74 mV) are thus termed 'high-RP cells', while those from the second population (mean at -41 mV) are referred to as 'low-RP cells'. About 52 ± 2% of the total sample were high-RP cells, with the remainder (48%) being the low-RP cells.

Several tests were carried out to address whether the low RP in a group of cells was due to mechanical reasons, such as preparations being partially damaged by dissection, or electrodes being poorly sealed with the membrane or localized in an isolated compartment of the cell. It was found that cells with low- and high-level RPs could usually be recorded simultaneously in the same preparations, physically quite close to each other (0.1–1 mm; Fig. 9*C*, $n = 13$), or consecutively only 1–2 min apart ($n > 10$). Many deliberate micrometre movements of the electrode in three axes resulted in either no significant change in the RP or dislocation from the cell, but never caused a fast change of the RP from one level to another. In addition, the input resistance of low-RP cells was 17.1 ± 6.88 MΩ ($n = 10$, Fig. 7*A*), which is about two times the value measured from high-RP cells (8.8 ± 4.52 MΩ, $n = 11$). Finally, many low-RP cells exhibited a long-lasting recording time (> 30 min, $n > 30$) and always responded to ACh or elevated extracellular K^+ concentration (high K^+) with a robust and reversible hyperpolarization (see below), suggesting a good quality of recording.

According to the time elapsed from vessel isolation to electrical recording (*in vitro* incubation time), these data from 771 cells were separated into two groups: one had an incubation time of 0.5–8 h (1st day cells, $n = 591$) and the other had an incubation time of 24–32 h (2nd day cells, $n = 180$). Analysis of each group revealed a bimodal distribution that closely resembled that from the combined data (Fig. 2*B*). The average (± S.D.) membrane potentials for the high- and low-RP cells did not differ significantly across days ($P > 0.05$ for each case, likelihood ratio test; Casella & Berger, 1990). However, the 2nd day preparation produced a significantly higher proportion of high-RP cells than the 1st day preparation. Of the cells in the 1st day preparation, 48% belonged to the high-RP group, compared to 69% of the cells from the 2nd day preparation ($P < 0.001$).

To define the individual cells in the RP classes, we used -57 mV as a convenient boundary, as the mixture function attains a minimum between the two peaks at -57 mV. This will theoretically lead to a misclassification of a small portion of the cells (0.8–1.3%) that fall into the overlapping area of the two Gaussian curves. Using this criterion, of 72 dye-identified cells, 17 and 32 SMCs, and 8 and 15 ECs belonged to the high- and low-RP classes, respectively (Fig. 2*C*). There were no significant differences between the mean values of high-RP, low-RP and the high-RP/low-RP ratio between the SMCs and ECs ($P > 0.05$ for each case).

The membrane properties of typical high- and low-RP cells are quite different, as described below. In these studies, we defined the cells as typical low-RP cells only when the RP was -50 mV or less negative, and cells were defined as typical high-RP cells only when the RP was more negative than -65 mV. The 'intermediate RP cells', which had RPs between -50 and -65 mV comprised approximately 13.8% of the total count. The properties of these cells were not studied systematically, but they

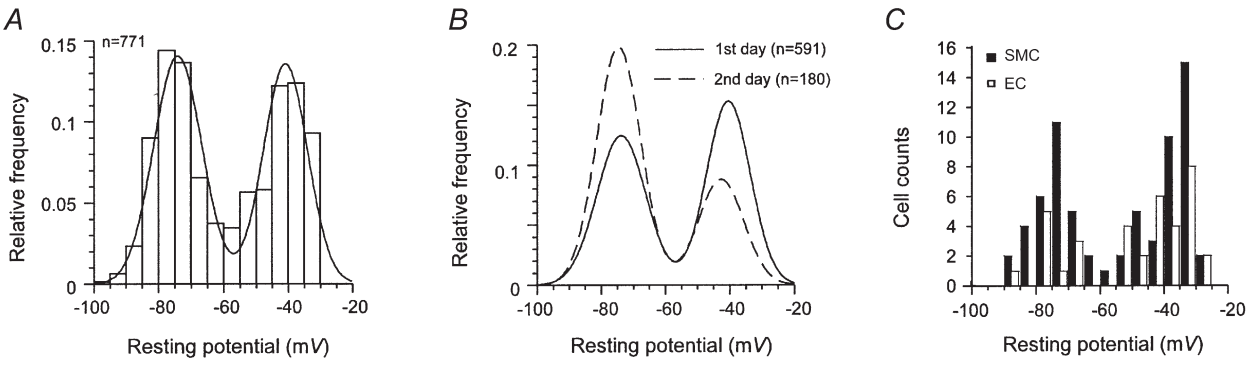

Figure 2. Two-peak Gaussian distribution of membrane RPs

A, this 5 mV bin histogram of a total of 771 cells shows a bimodal distribution. The RP data are modelled as a mixture of two Gaussian density functions (curve), peaking at means of -41 and -74 mV, revealing two populations, called 'low-RP' and 'high-RP' cells, respectively. The population ratio of low-RP/high-RP cells is 0.48/0.52. *B*, the effects of preparation incubation time on the RP distribution. Density curves are based on data from the preparations incubated for less than 8 h (1st day, continuous line) and those incubated for 24–32 h (2nd day, dashed line). The low-RP/high-RP population ratio of the 2nd day preparations was significantly lower than that of the 1st day preparations. *C*, RP histograms of dye-identified SMCs and ECs show a similar two-peak distribution.

seemed indeed to show transitional properties between those of high- and low-RP cells (see below).

Responses of the high- and low-RP cells to high K^+

Membrane potential responses to elevated $[K^+]_o$ (high K^+) were strikingly different between the low-RP and high-RP cells (Figs 3 and 4). In high-RP cells, high K^+ (7.5–50 mM) caused a concentration-dependent depolarization ($n = 98$). Figure 3*A* and *B* shows an example in which the membrane potential levels were almost linearly related to the logarithmic value of $[K^+]_o$. Assuming the K^+ permeability is solely responsible for the RP, a Nernst equation (at 35 °C) fitted to the four data points resulted in a $[K^+]_i$ estimation of 119 mM and a K^+ equilibrium potential (E_K) of −84 mV (Hille, 1992). By using the same method, the calculated $[K^+]_i$ was 131 and 125 mM and the E_K was −87 and −86 mV in two other cells.

On the other hand, 7.5–20 mM K^+ caused a hyperpolarization in 38 out of 42 low-RP cells (Fig. 4). The remaining cells showed either a 2–10 mV depolarization ($n = 3$) or no response ($n = 1$). Application of a solution containing 30 mM K^+ or higher often produced a brief hyperpolarization followed by a depolarization beyond the control membrane potential ($n = 6$). A cumulative application of incrementally higher $[K^+]_o$ caused a hyperpolarization only at the wash-in of the first high K^+ solution (Fig. 4*B*). The other high K^+ solutions each produced a depolarization to its immediately previous potential level. It is interesting to note the onset and the offset of the high K^+-induced hyperpolarization. With a small $[K^+]$ increase (7.5–10 mM), the onset of hyperpolarization was often tri-phasic: slow at the beginning; after a turning point, it became very fast (7.2 ± 1.1 mV s^{-1}, $n = 11$); and later a slow hyperpolarization (Fig. 4*A*, labels 1, 2 and 3). The slow-to-fast turning point was at −40 to −45 mV ($n = 20$). With a medium or high molar $[K^+]$ (20–50 mM), the beginning slow onset phase was brief or even unnoticeable.

Ba^{2+} (10–500 μM) depolarized all of the high-RP cells ($n = 78$, Fig. 3*C*) to a level between −40 and −25 mV and increased the input resistance (also see Jiang *et al.* 1999), but only slightly depolarized the low-RP cells when 50 μM Ba^{2+} was applied (6.8 ± 0.63 mV, $n = 8$). In the presence of Ba^{2+} (10–50 μM), 10 mM K^+ caused either a small hyperpolarization (2–12 mV) or no potential changes in low-RP cells (not shown) and in the Ba^{2+}-predepolarized high-RP cells ($n = 4$ and 7, respectively; Fig. 3*C*), suggesting a key role of the K_{ir} channel in the generation of the high K^+-induced hyperpolarization. In two cells with an intermediate RP (−60 and −62 mV), 10 mM K^+ caused a depolarization of 0 and 2 mV, respectively.

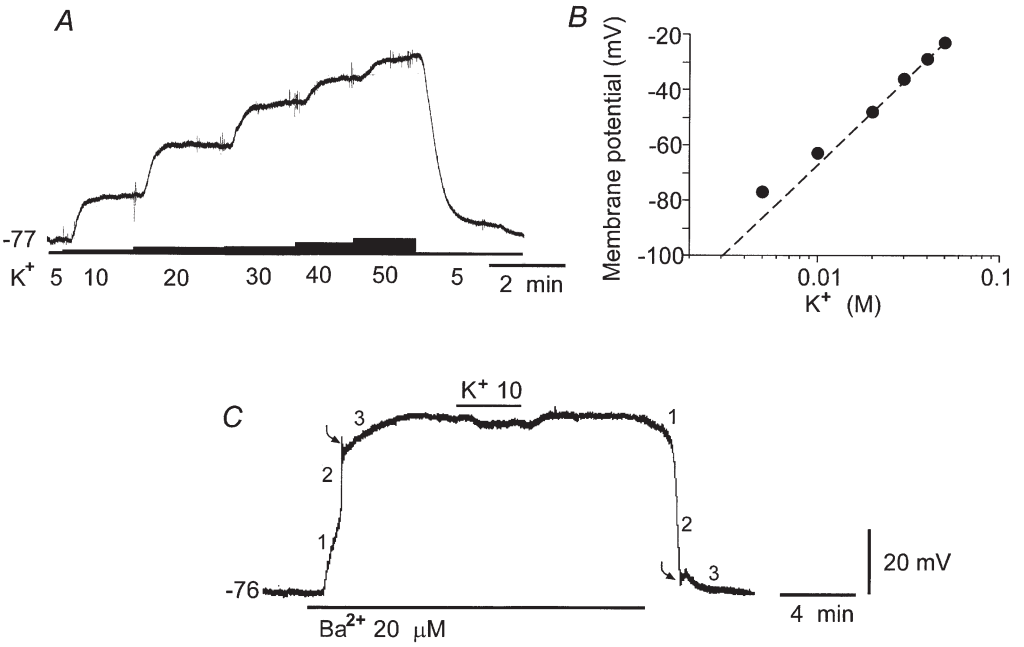

Figure 3. Effects of high K^+ on the membrane potential of a high-RP cell

A, a sample chart record of the RP that was depolarized in a concentration-dependent manner by high K^+ in the bathing solution. The concentrations of K^+ (mM) applied are indicated by bars below the trace. In this and the following figures RPs are in mV. *B*, a semi-logarithmic plot of the voltage–K^+ concentration relationship data from *A*. The dashed line represents a Nernst function fitted to the four data points on the right, revealing an $[K^+]_i \geqslant 119$ mM. *C*, elevated $[K^+]_o$ caused a small hyperpolarization in a high-RP cell that was depolarized by Ba^{2+} (20 μM). Note that there is a fast phase (2) and an overshot (curved arrows) between early (1) and late (3) slow phases in both onset and offset courses of the barium-induced depolarization. *A* and *C* are from different cells. The voltage scale bar in *C* also applies to *A*.

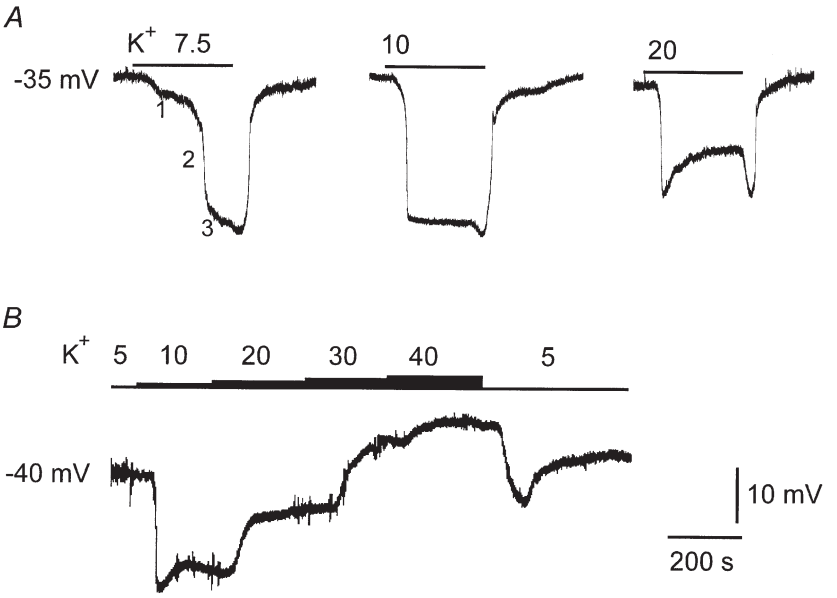

Figure 4. High K^+ actions on the membrane potential of low-RP cells

A, medium elevations of $[K^+]_o$ (mM) caused reversible hyperpolarizations in a low-RP cell. Note the triphasic onset (1, 2, 3) at the wash-in of 7.5 mM K^+. *B*, a cumulative increase in $[K^+]_o$ (mM) induced a hyperpolarization only at the first increment. The subsequent increments in $[K^+]_o$ caused depolarizations to its immediately prior level. *A* and *B* are from different cells. Scale bars apply to both *A* and *B*.

Responses of high-RP and low-RP cells to ACh

Membrane responses to ACh were also different between the high- and low-RP cells (Fig. 5). In high-RP cells, ACh (0.1–10 μM) always caused a concentration-dependent depolarization ($n = 15$; Fig. 5*A*). The ACh-induced depolarization was usually slow in onset and offset, but a fast peak followed by a slow depolarization or other variable shapes were frequently seen (Fig. 5*C*). The peak amplitude of depolarization induced by 10 μM ACh was 9.7 ± 2.2 mV ($n = 17$), and ranged between 3 and 33 mV.

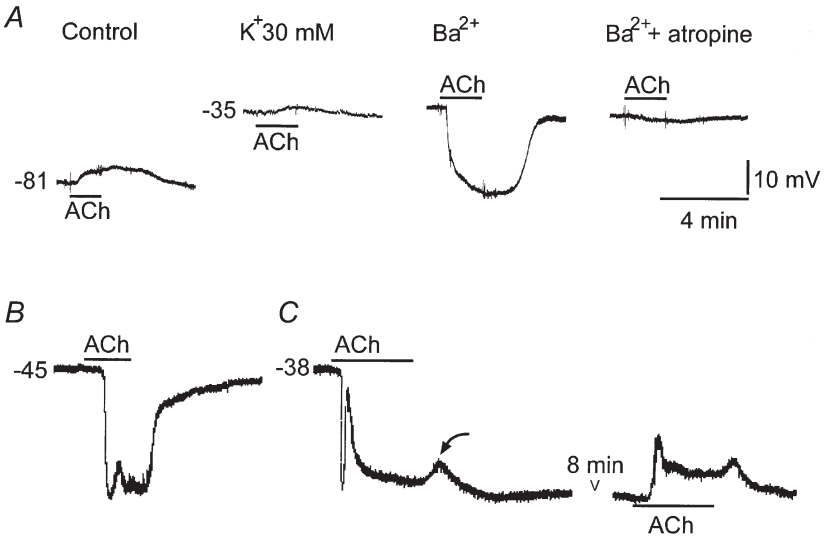

Figure 5. Depolarization and hyperpolarization by ACh in high-RP and low-RP cells

A, under control conditions, ACh (10 μM) depolarized a high-RP cell, whereas when the cell was depolarized by 100 μM Ba^{2+}, ACh caused the cell to hyperpolarize; when predepolarized by high K^+, the ACh-induced depolarization was reduced. The ACh-induced hyperpolarization was blocked by atropine (1 μM). The control levels of the traces, with the exception of the first (−81 mV), are shown in accordance with the scale. *B*, ACh reversibly hyperpolarized a low-RP cell. *C*, the recovery of the ACh-induced hyperpolarization following wash-out of ACh in this particular case aborted (curved arrow). The RP further shifted to a stable level of −74 mV. At the latter status, ACh depolarized the cell.

The ACh-induced depolarization was reduced by 50–70 % when the cells were depolarized to about −30 mV by 30 mM K^+ ($n = 4$; Fig. 5*A*). The ACh responses, including the hyperpolarization in low-RP cells described below, were all blocked by 1 μM atropine.

In low-RP cells, ACh (0.1–10 μM) induced a robust hyperpolarization in all of the cells tested ($n = 25$). The amplitude of hyperpolarization induced by 1 and 10 μM ACh was 22.4 ± 2.5 mV ($n = 9$) and 30 ± 2.2 mV ($n = 8$), respectively. The ACh-induced hyperpolarization usually showed a fast phase in the wash-in onset and the wash-out offset. A fast notch was often seen at the beginning of the ACh-induced response, which divided the latter into a fast early hyperpolarization and a late sustained hyperpolarization ($n = 6$; Fig. 5*B* and *C*). When the membrane potential of a low-RP cell shifted to a high level near the high-RP mean of −74 mV (Fig. 5*C*, and see below for details), the membrane response to ACh always became a depolarization ($n = 10$). The amplitude and waveform of the ACh-induced depolarization in these cells were not significantly different from those seen in the originally high-RP cells. It was noted that the peak of the ACh-induced depolarization often reached a level that was less negative than the maximum level of the hyperpolarization in the same cell (Fig. 5*C*, $n = 4$), suggesting that the observed ACh-induced depolarization and hyperpolarization do not fit into a single voltage-dependent reversal phenomenon; rather they probably involve different ionic mechanisms.

When the high-RP cells were predepolarized to about −40 to −25 mV by Ba^{2+} (10–500 μM), ACh also induced a robust hyperpolarization in 35 of the 38 cells tested (Fig. 5*A*), and a small (1–5 mV) depolarization in the remaining 3 cells. The amplitude of the hyperpolarization induced by 1 and 10 μM ACh was 16.6 ± 5.0 mV ($n = 7$) and 24.4 ± 1.3 mV ($n = 9$), respectively (Fig. 6). These were not significantly different from the ACh response induced in the originally low-RP cells without the presence of Ba^{2+} ($P > 0.6$, Student's t test). The fast onset, offset and the notch were also seen in ACh-induced hyperpolarizations in the Ba^{2+}-predepolarized high-RP cells ($n = 6$), but these features were usually less prominent (Fig. 5*A*). ACh (10 μM) induced a small depolarization (< 2 mV, $n = 3$) and hyperpolarization (< 5 mV, $n = 2$) in the cells that had an 'intermediate' RP of −58 to −62 mV.

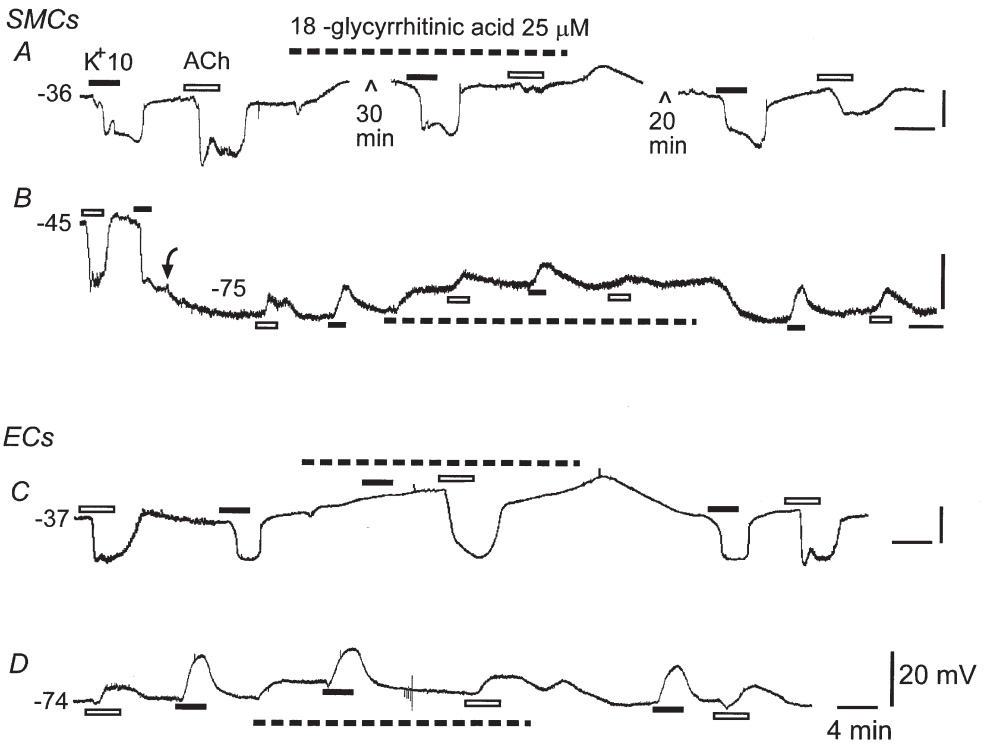

Figure 6. ACh-induced hyperpolarization in SMCs, but not in ECs, suppressed by gap junction blockade

Sample records *A* and *B* are from dye-identified SMCs, and those in *C* and *D* are from ECs. Note that *A* and *C* are from low-RP cells, whereas *B* and *D* are from high-RP, or initially low- but shifted to high-RP cells (curved arrow). ACh-induced hyperpolarization was almost completely abolished by 18β-glycyrrhetinic acid (18βGRA) in the SMC (*A*), but not in the EC (*C*). The ACh-induced depolarization of the SMC (*B*) but not that of the EC (*D*) was partially inhibited by 18βGRA. Note also that high K^+-induced hyperpolarization in the EC (*C*) was abolished by 18βGRA. 18βGRA itself depolarized the cells. All of the effects of 18βGRA were reversible after wash-out for 10–20 min.

Responses of SMCs *vs.* ECs to high K^+ and ACh

Dye-identified SMCs and ECs showed similar high K^+ and ACh response patterns to those described above, depending on their membrane potential levels, that were indistinguishable between the two cell types (Fig. 6). In SMCs, 18βGRA (25 μM), a putative gap junction blocker (Yamamoto *et al.* 1998), almost completely suppressed the ACh-induced hyperpolarization ($84.6 \pm 4.2\%$, $n = 4$, Fig. 6*A*) and significantly reduced the ACh-induced depolarization ($72.6 \pm 6.4\%$, $n = 5$, Fig. 6*B*), but had no effect on the ACh responses in the ECs ($n \geqslant 4$, Fig. 6*C* and *D*). On the other hand, the high K^+-induced hyperpolarization in ECs ($n = 3$, Fig. 6*C*), but not in SMCs, was blocked by 18βGRA. The compound 18βGRA itself caused a reversible depolarization in both SMCs and ECs of either RP level (10.8 ± 0.9 mV, $n = 13$), which is expected to enhance the driving force for the ACh-induced hyperpolarization (Fig. 6*C*; also see Coleman *et al.* 2001). 18βGRA caused a RP shift from the high to the low level in two ECs, but not in six other ECs. No RP level shifts were observed in the SMCs. These data support the notion that the ACh-induced hyperpolarization originates in ECs (i.e. the SMC membrane hyperpolarization induced by ACh is a spread of the EC response via electrically coupled channels; Yamamoto *et al.* 1998; Coleman *et al.* 2001), whereas the high K^+-induced hyperpolarization may originate from the SMCs.

Shift from the low-RP state to the high-RP state

A shift of the membrane potential of low-RP cells to a high negative level (−65 to −85 mV) for the remaining period of the recordings (10–120 min) was frequently observed (Figs 5*C*, 6*B* and 7). A spontaneous shift from the low-RP to a permanent high-RP level was observed in 27 cells after 8–67 min of initial recording (Figs 7*E* and 9*C*). Such a shift was swift in its course, slower at the onset and the end, but fast in the middle phase, with an entire time course of about 4–7 min. The shift was more often triggered by a hyperpolarization caused by a 2–3 min application of high K^+ (10 mM; $n = 48$) or by ACh (1–10 μM; $n = 26$). In these cases, the wash-out recovery of the membrane potential was either aborted (Figs 5*C*, 6*B* and 7*A*) or not seen (Fig. 7*C* and *D*). Rather, the RP further shifted to and stayed at a level near −74 mV in the remaining recording period. The input resistance of three cells was reduced to 6.2, 8.7 and 11.6 MΩ from the control levels of 16.0, 18.1 and 17.8 MΩ, respectively (Fig. 7*A*).

The triggered shift was also observed after a brief (2–3 min) application of other hyperpolarizing compounds (Fig. 7*C* and *D*), such as the nitric oxide (NO) donor DPTA-NONOate (10 μM; $n = 3$) and the K_{ATP} channel opener pinacidil (10 μM; $n = 4$). A membrane-permeable form of cAMP, 8-bromo-cAMP (1 mM), caused a reversible small

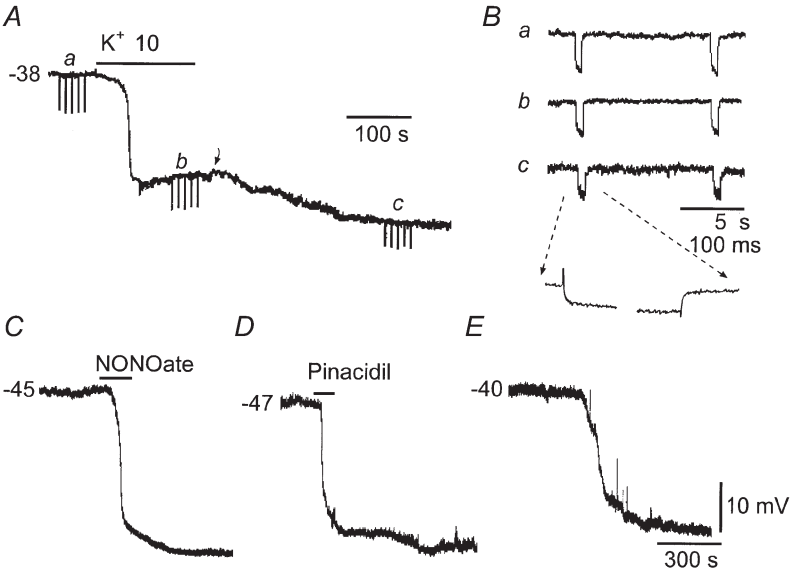

Figure 7. Shifting from a low-RP state to a high-RP state

A, an example cell showing that an application of high K^+ (10 mM) caused a non-reversible shift from a low-RP state to a high-RP state. The recovery following the high K^+ washout was aborted (curved arrow). The downward deflections at *a*, *b* and *c* are the electrotonic potentials induced by rectangular transmembrane current pulses (−0.4 nA, 1 s). They are further shown in *B* on an expanded time scale, indicating an input resistance of 17.8, 16.0 and 11.6 MΩ at *a*, *b* and *c*, respectively. The bottom trace is the five sweep-averaged trace of *c* with the time scale further expanded showing the bridge balance example. *C*–*E*, example of cells undergoing low- to high-RP shifts due to a hyperpolarization induced by the nitric oxide donor DPTA-NONOate (10 μM; *C*), the ATP-sensitive K^+ channel activator pinacidil (100 μM; *D*) and an unknown spontaneous reason (*E*). The voltage scale bar applies to all traces. The 300 s time scale bar applies to *C*–*E*.

hyperpolarization (2–5 mV) in low-RP cells ($n = 4$) and never induced a permanent shift to the high-RP level.

Shift from the high-RP state to the low-RP state

Ba^{2+} (1–500 μM) caused a robust depolarization in high-RP cells to a low level from −50 to −25 mV (also Jiang *et al.* 1999). The depolarization induced by 1–50 μM Ba^{2+} was usually completely reversible after a 5–10 min wash (Fig. 3*C*). When a low concentration (1–50 μM) was used, the Ba^{2+} wash-in depolarization and wash-out repolarization were clearly tri-phasic: a fast phase and an overshoot appeared between an early and a late slow phase (Figs 3*C* and 8*A*), indicating that a regenerative process occurred in the mid-phase. The threshold for appearance of the fast depolarization was -63 ± 1.2 mV ($n = 7$, 50 μM Ba^{2+}). Moreover, in four cells, the RP shifted from a high level (−71 to −85 mV) and remained at a level of approximately −40 mV in the remaining 25–45 min recording time after the 50 μM Ba^{2+} washout.

A shift from a high-RP state to a permanent low-RP state was occasionally observed in other cases (Fig. 8). A depolarization induced by the Na^+–K^+ pump current inhibitor ouabain (100 μM) in high-RP cells was often large (32.8 ± 1.8 mV, $n = 10$) and fully reversible after a 15 min wash. However, in four cells, the RP remained at a low level (approximately −40 mV) after 24–55 min washout. A permanent shift to the low-RP level in two high-RP cells was triggered by large consecutive excitatory junction potentials (EJPs) induced by perivascular stimulation (Hirst & Edwards, 1989; Jiang *et al.* 1999). On the other hand, an application of Rp-cAMPS (10–20 μM), 4AP (1–10 mM), glipizide (1–10 μM), charybdotoxin (50–100 nM) and apamin (50–100 nM) all caused either a small depolarization (1–5 mV) or no membrane potential change in high-RP cells ($n \geqslant 4$), but never caused a shift to the low-RP level. These compounds each caused a 3–10 mV depolarization in the low-RP cells ($n \geqslant 4$). A spontaneous shift from a high-RP state, either of an initially high-RP cell or of cells that had shifted to this level from a low-RP level, to a permanent low-RP state was recorded only infrequently ($n = 4$; Fig. 8*D*). A spontaneous oscillation between −75 and −39 mV was observed in three short-lived cells.

The responses to high K^+ and ACh of the cells that had shifted from high- to low-RP states, with or without Ba^{2+} present, were almost always hyperpolarizations (Figs 3*C*, 5*A*, and 8*B* and *C*). However, the amplitude and the onset and offset speeds of the hyperpolarization caused by 10 mM K^+ in cells with Ba^{2+} present (Fig. 3*C*) were much lower than those seen in low-RP cells without the presence of Ba^{2+} (Figs 4, 6*A* and *C*).

In dye-identified cells, a low- to high-RP shift was observed in ECs ($n = 9$) as well as in SMCs ($n = 7$, Fig. 6*B*) after a brief application of ACh or high K^+. A high- to low-RP shift was seen in two of six ECs after 18βGRA administration.

Electrical coupling *vs.* the two RP levels

Simultaneous intracellular recording of two cells was conducted to detect the coexistence of the two distinct levels of RP and to estimate the intensity of electrical coupling between the cells in the proximal SMA segments (3–5 mm long, Fig. 9). Dual cells 0.2–1.0 mm apart showed initial low–low, high–high and high–low-RPs in 20, 19 and 13 pairs, respectively. The cells in dual-cell recording

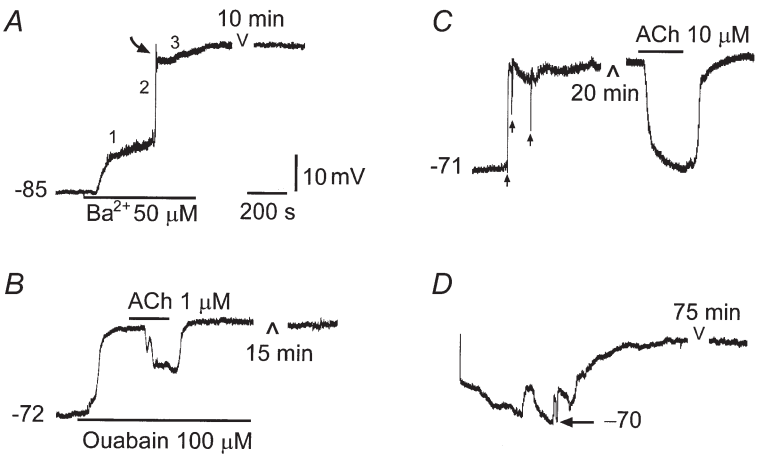

Figure 8. Shifting from a high-RP to a low-RP state

A, Ba^{2+} caused a non-reversible RP shift from a high to a low level in this cell. Note the three phases (1, 2, 3) of depolarization and the lack of wash-out recovery. *B*, a high- to low-RP shift induced by a 15 min application of ouabain, an inhibitor of the electrogenic Na^+–K^+ pump. *C*, a high- to low-RP shift triggered by three excitatory junction potentials evoked by perivascular nerve stimuli (arrows, 40 V, 0.4 ms). *D*, a cell undergoing a spontaneous shift from the initial, unstable high-RP state to a long-lasting low-RP state. Note that the cells always showed a hyperpolarizing response to ACh when they shifted to the low-RP status (*B* and *C*).

conditions had a pattern of response to ACh or high K^+ that was not different from those seen in the single-cell recording mode described above (Fig. 9*C*; i.e. dependent upon the RP level of individual cells). The electrotonic potential induced by a current pulse of up to 1.5 nA was detected not only in the current-injected cell, but also in the majority of non-injected cells when the pair of cells had a separation distance of $\leqslant 0.7$ mm (14 out of 18), indicating the existence of electrical coupling. No electrotonic potential was detected in the non-injected cell when it was $\geqslant 0.8$ mm away from the current-injected cell ($n = 6$). The coupling ratio, defined as the amplitude of the electrotonic potential of the non-injected cell divided by that of the injected cell, was estimated to be 0.03 ± 0.01 for a separation distance of 0.34 ± 0.02 mm (range 0.2–0.4 mm, $n = 13$). The coupling ratio was 0.021 ± 0.01 ($n = 3$), 0.058 ± 0.038 ($n = 3$) and 0.013 ± 0.004 ($n = 7$) for low–low, high–high and low–high RP pairs, respectively. No statistical significance was found for the mean differences ($P > 0.3$, Student's t test). The recorded pairs were identified as SMC–SMC, SMC–EC and EC–EC combinations ($n > 3$ each), but no efforts were made to compare the coupling ratios between the different combinations because, based on the cellular architecture of the arterioles (Sandow & Hill, 2000), all three coupling combinations are likely to be included in the current pathway between each pair of cells recorded with such separation distances.

DISCUSSION

Low RP is a functional state, rather than a mechanical artifact

The low RP in nearly half of the cells sampled is unlikely to be an artifact due to a mechanical injury or a less-than-ideal electrode tip localization for the following reasons. (1) High-RP and low-RP cells could be recorded simultaneously or consecutively in the same preparation within 0.1–0.2 mm, which would be unlikely if part of the vessel were injured by dissection. (2) The low-RP cells can maintain a RP level near −40 mV for more than 2 h, during which time robust reversible hyperpolarizing responses to high K^+ and ACh (Figs 4, and 6*A* and *C*) were observed, indicating a high quality of recording. (3) The input resistance of low-RP cells was about double that of the high-RP cells in the same preparation. A mechanically injured cell or one poorly sealed with the electrode is expected to be leaky at its membrane and have a low input resistance. (4) Randomly sampled cells showed a bimodal Gaussian distribution rather than a single Gaussian distribution, with a base skewed in the less negative direction. The latter would have been expected if variable degrees of penetration injury or an imperfect seal did cause a reduction in the RP. (5) Many examples of fast shifts between the low- and high-RP levels support the concept that a RP at the intermediate level (−50 to −65 mV) is usually unstable, tending to move to either

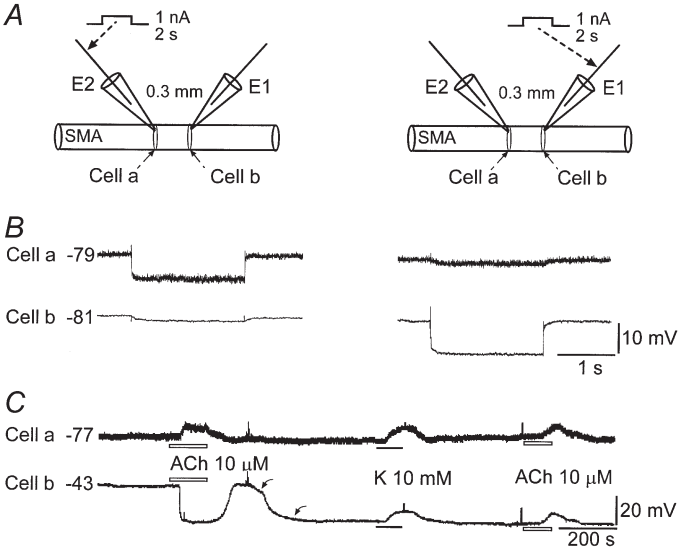

Figure 9. Dual cell membrane potential recordings from the SMA

A, this schematic drawing of the experimental settings for *B* depicts the current pulse injection (1 nA, 2 s) into either cell (electrode (E)2 for cell a, and E1 for cell b) by balanced bridge mode. The SMA segment was 5 mm long. *B*, the current induced a large electrotonic membrane potential in the injected cells (left, 9.8 mV in cell a; right, 11.6 mV in cell b) while producing a small electrotonic potential in the other cell, revealing a coupling ratio of 14 and 13 % in left and right cases, respectively. Note that the traces of cell b, but not of cell a, were low-pass (3 kHz) filtered. All traces are an average of three sweeps. *C*, another pair of cells 0.5 mm apart initially exhibited a high RP (cell a) and a low RP (cell b) and different responses to ACh. After a shift of RP from a low to a high level (curved arrows) in cell b, the two cells showed similar responses to 10 mM K^+ and ACh.

the low or high levels. (6) Micrometre movement of the electrode never caused a fast shift of the RP from one state to another. This renders it unlikely that a low RP is due to poor electrode localization. Taken together, we may rule out the possibility that a mechanical factor caused an artifactually low RP in a group of cells sampled. Instead, in addition to the group of SMCs that have a stable high RP, there exists a group of cells that have a stable low RP in the *in vitro* SMA preparation.

As spontaneous and neurohumoral-evoked shifts between low- and high-RP levels were often encountered, low- and high-RP cells seem to be anatomically indistinct, in contrast to the case of the striatum where a cholinergic neuron group with low RPs is cytologically distinguishable from the GABAergic high-RP principal cells (Jiang & North, 1991). The dye-identified SMCs and ECs both having two levels of RP further supports the idea that most, if not all, cells in the *in vitro* SMA appear to have two exchangeable resting states; when the neurohumoral environment of the vessel changes, the proportion and distribution of the cells in the two states may vary. Interestingly, the mean RP level of the low-RP cells (−41 mV) is very close to what has been found in arteries pressurized to about 60 mmHg (Dietrich & Dacey, 1994; Knot & Nelson, 1995), and arteries in *in vivo* conditions (Welsh & Segal, 1998). We also observed that low-RP cells were more prevalent in newly dissected tissue (1st day preparation), while significantly more high-RP cells were seen in the 2nd day preparation. This evidence seems to suggest that in the SMA, the low-RP state, rather than the high-RP state, is closer to the natural physiological status.

Role of K_{ir} in setting the two RP states

The high-RP level near −74 mV is likely to be due to highly activated K_{ir} channels in these cells, whereas the low-RP level is due to a lack of K_{ir} activation. The high-RP cells had a situation similar to that found in guinea-pig submucosal arterioles and the proximal segments of rat cerebral arterioles *in vitro* (Edwards & Hirst, 1988; Edwards *et al.* 1988). In addition to our previous report that the current–voltage relationship in the high-RP cells always showed an inward rectification (Jiang *et al.* 1999), the present results showed that: (1) 1–50 μM Ba^{2+}, a concentration that selectively blocks the K_{ir} (Hirst & van Helden, 1982; Quayle *et al.* 1997), caused a consistent large depolarization reaching the low-RP level near −41 mV, (2) the barium-induced depolarization showed a regenerative fast time course in its onset and offset, which is what can be expected from the voltage-dependent feature of this channel, and the channel is the dominating conductance in a cell, although a role for a voltage-dependent Ca^{2+} channel in the regenerative depolarization remains to be excluded, and (3) the high-RP cells had a lower input resistance than the low-RP cells, but this input resistance could be raised by Ba^{2+} to that of the low-RP cells (Jiang *et al.* 1999). Taken together, our data support the idea that K_{ir} is highly activated in the high-RP cells under *in vitro* baseline conditions.

The lack of K_{ir} activation in low-RP cells is evidenced by the following results. First, these cells had a RP near −41 mV, which is far less negative than the reported activation threshold for K_{ir} in an $[K^+]_o$ of 5 mM (Edwards *et al.* 1988; Hirst & Edwards, 1989). Second, Ba^{2+} (50–100 μM) caused only a small depolarization in these cells. Third, elevation of $[K^+]_o$ induced a robust hyperpolarization in these cells, and that hyperpolarization showed a regenerative fast time course, suggesting a large availability for K_{ir} activation in the low-RP state. The high K^+-induced hyperpolarization can be interpreted to mean that elevated $[K^+]_o$ causes a relief of Mg^{2+} block and thus activation of K_{ir} (Doupnik *et al.* 1995). The membrane potential would then move towards the E_K, which is estimated to be more negative than −67 and −49 mV in 10 and 20 mM K^+, respectively (Hille, 1992). In this respect, it has been reported that in dispersed single SMCs, an elevation of $[K^+]_o$ causes augmentation of the maximum K_{ir} conductance and a shift of the K_{ir} activation voltage towards a less negative value (Quayle *et al.* 1996). Finally, when low-RP cells shifted to a high-RP state, 50–100 μM Ba^{2+} depolarized them to a level comparable to that of the low-RP cells.

Several other ionic channels have been reported to contribute to the resting membrane conductance of arterial SMCs and ECs. Our result showed that 4AP, glipizide, apamin and charybdotoxin all induced a depolarization in low-RP cells, whereas they had little effect on high-RP cells. This suggests that under basal conditions, K_{DR}, K_{ATP} and K_{Ca} each play a minor role in maintaining the RP, but have little contribution to the setting of the high-RP state. The non-voltage-dependent K^+ ($K_{non\text{-}V}$) channel in renal arcuate artery is partially sensitive to Ba^{2+} (> 100 μM) but not to any known K^+ channel blockers (Prior *et al.* 1998). This makes it difficult to assess its role in the setting of the low-RP state in our preparation, but the channel seems to provide little contribution to the high-RP state because 10–50 μM Ba^{2+} was often sufficient to depolarize the cells to beyond −41 mV. Ouabain caused a significant depolarization or a shift to the low-RP state in high-RP cells (Fig. 8*B*). A plausible interpretation seems to be that the pump current is an important element that assists the maximum activation of the K_{ir} rather than itself setting the high RP, because when K_{ir} is blocked by Ba^{2+}, abnormal activation of the pump by high K^+ never caused a shift of the RP back to the high level (Fig. 3*C*). Finally, the role of stretch-activated channels in the setting of the RP level remains to be tested. This mechanically sensitive channel has a reversal potential near −15 mV (Setoguchi *et al.* 1997). It is possible that the unpressurized condition of our vessel preparation might have deactivated this cation channel, which permitted a full activation of the K_{ir} and thus caused a high-RP level.

Nonetheless, it is obvious that K_{ir} remains the key element in the setting of the high-RP level.

Moreover, it appears that the original low-RP and high-RP cells may have similar amounts of K_{ir} channel molecules because the great majority of originally low-RP cells in our study showed a hyperpolarization response to high K^+, and some of them could shift the RP to a level not different from that of the original high-RP cells. However, the high K^+-induced hyperpolarization in ECs is blocked by 18βGRA, suggesting that at least some of the ECs in the SMA express fewer or no K_{ir} channels, or that their K_{ir} is less sensitive to $[K^+]_o$ elevation. Consistent with this notion, we did find that two ECs shifted their RP from a high level to the low level after 18βGRA application.

What makes K_{ir} stay non-activated or activated?

Keeping K_{ir} non-activated in low-RP cells under baseline conditions appears simple: the cell's much less negative RP will itself result in a great Mg^{2+}/polyamine block to the channel (Doupnik *et al.* 1995), while the membrane potential is determined according to the Goldman-Hodgkin-Katz equation by other K^+ channels, Na^+, Ca^{2+} and Cl^- conductances and the ionic concentrations on both sides of the cell membrane (Hille, 1992). However, a barium-induced depolarization to or beyond the level of −41 mV usually recovered completely to the control level of a high-RP cell upon Ba^{2+} washout, suggesting that depolarization alone is not sufficient to prevent K_{ir} from reactivating after wash-out of Ba^{2+}.

A permanent shift from a low- to a high-RP state can be triggered by the K_{ir} and Na^+–K^+ pump activator high K^+, the K_{Ca} activator ACh (Jiang *et al.* 2001) and the K_{ATP} activators pinacidil and NO (Si *et al.* 2001). Since these triggers have in common a large membrane polarization, it seems to suggest that the hyperpolarization itself is a key factor to invoke the maximal K_{ir} activation and keep it activated. This is consistent with the unique voltage dependency of this channel: suprathreshold hyperpolarization opens the channel and thus increases the efflux of K^+ ions. The voltage and the increased extracellular K^+ ion cause further K_{ir} channel opening, Na^+–K^+ pump activation and thus hyperpolarization (Edwards *et al.* 1998). This positive feedback or regenerative process will continue until the membrane potential moves near E_K, where a net K^+ flux becomes zero. Once a RP is hyperpolarized near E_K by the dominating K_{ir}, any minor alteration of K^+ conductance will become ineffective in changing the membrane potential because of the small driving force for K^+. Hyperpolarization also deactivates voltage-dependent Ca^{2+} channels in the vascular SMCs (Nelson *et al.* 1990; Knot & Nelson, 1998). Taken together, it seems reasonable that fully activated K_{ir} and the high RP form a state with good stability. However, in many cases, an induced regenerative hyperpolarization in the low-RP cells recovered to control levels upon wash-out of the agents (e.g. K^+, ACh), suggesting that a hyperpolarized membrane potential alone is not sufficient to keep the K_{ir} activated. One may argue that the recovery is due to the hyperpolarization not being large enough. This is not often the case (Figs 5*B* and 8*C*); moreover, in cells that shift spontaneously from a low-RP to a high-RP state (Fig. 7*E*), no pre-shift hyperpolarization seemed to have been required.

Taken together, there must be some factor(s) assisting or inhibiting the activation of K_{ir}, or some modulating process(es) directly regulating the activation or inactivation of K_{ir}. This is further supported by our data that the 2nd day SMA preparations contained more high-RP cells than the 1st day preparations. In this respect, the second messengers cAMP and cGMP have been implicated in the positive modulation of vascular K_{ir}, K_{ATP}, K_{DR} and K_{Ca} via protein phosphorylation (Schubert *et al.* 1996; Wellman *et al.* 1998; Feletou & Vanhoutte, 1999). Application of 8-bromo-cAMP failed to cause a shift from the low-RP to the high-RP state. Furthermore, the protein kinase I and II inhibitor Rp-cAMPS failed to shift cells from a high-RP to a low-RP state, suggesting that the cAMP-dependent protein phosphorylation pathway does not play a significant role in the shifting or maintenance of the RP state. Several other tonic RP-regulating mechanisms, such as cytosolic levels of cGMP, Na^+ and Ca^{2+}, stretch-activated channels, and the electrogenic Na^+–K^+–ATP pump remain to be investigated.

Two RP states *vs.* electrical coupling

The simultaneous existence of two distinct levels of RP in SMA cells that are physically close to each other extended the observations that the RP in guinea-pig heart arterioles also shows a bimodal distribution that peaks at −23 and −61 mV (Klieber & Daut, 1994). It is a general concept that the steady-state membrane potentials of the cells in an electrically well-coupled tissue are uniform, and the length of arteries or arterioles can be treated as an electrical cable with a length constant (λ) of 0.3–1.5 mm (Hirst & Edwards, 1989). Our observations raised the question of how well the SMCs and the ECs in the SMA are electrically coupled. The multiple EC labelling (Fig. 1*B*), the reciprocal spread of electrotonic potentials in dual-cell recording (Fig. 9), the myoendothelial spread of the evoked EJP (seen in almost all cells recorded; Jiang *et al.* 1999), and the endothelio-muscular conduction of ACh-induced hyperpolarization (Fig. 6) all indicate that the SMCs and the ECs in the SMA are electrically coupled. However, our data indicate that the coupling strength is heterogeneous and rather poor in the SMA. First, we found that the coupling ratio between two cells that were ~0.3 mm apart was about 0.03, which is substantially smaller than what would expected from the reported λ values (0.37–0.82; Hirst & Edwards, 1989) in lengthy vessel segments ($\geqslant 4\lambda$ on each side of the current-injecting electrode). In short vessel segments (e.g. $\leqslant 1\lambda$), based on the cable theory, even higher coupling ratios should be expected (Hirst & Neild, 1978). Second, in four pairs of

cells that were 0.3–0.4 mm apart, a zero coupling ratio was detected, indicating that a coupling heterogeneity exists in the SMA. Finally, a voltage-gating of the gap junction channel conductance has been reported in a number of tissues or cultured cells (He *et al.* 1999). It is possible that a large voltage gradient between the low- and high-RP cells may also play a role in reducing the intercellular conductance at the high-RP/low-RP cell interfaces. Taken together, our data suggest that the cells in the SMA are poorly and heterogeneously coupled, and caution needs to be taken when using the electrical cable theory to predict the voltage distribution in arterioles like the SMA. For instance, Weidelt *et al.* (1997) also reported that the cells in rat small mesenteric arteries are poorly or even not electrically coupled.

Functional significance

The finding that there are two levels of RP set by all-or-none-like activation of K_{ir} in the vascular SMCs may have physiological and/or pathological significance. Such all-or-none behaviour of the K_{ir} in the SMA suggests that this channel forms the dominating resting conductance in the high-RP state and that it plays an enhanced role in the regulation of $[K^+]_o$ and in the autoregulation of cochlear blood flow. It has been demonstrated that K_{ir} plays an important role in the regulation of these parameters in the cerebral and coronary circulation (Edwards *et al.* 1988; Knot *et al.* 1996). The reported gain of autoregulation in the guinea-pig cochlea is 0.76 (Brown & Nuttall, 1994) *vs.* 0.14–0.38 in normal rat cerebral blood vessels (Osol & Halpern, 1985), which seems to be consistent with this contention. If this is true, it would be interesting to determine whether K_{ir} is also a dominating resting conductance in coronary and kidney arteries, and whether the cells there have bi-stable RP levels, since these vessel beds also have a high gain (0.7 and 0.81, respectively) in autoregulation (Tani *et al.* 1990; Hinojosa-Laborde *et al.* 1991). The bimodal RP distribution in guinea-pig heart arterioles supports this hypothesis (Klieber & Daut, 1994).

In conclusion, the RPs of the SMCs and ECs in the guinea-pig *in vitro* SMA are not uniform, but instead are composed of two stable levels near −40 and −75 mV. The RP level is set mainly by activation (−75 mV) and lack of activation (−40 mV) of the K_{ir} channel. Cells at one RP level may shift to another RP level in response to a change in the cellular environment, but the subcellular mechanism underlying such a shift and maintenance of the RP levels remains uncertain. This membrane property may have significance in neurohumoral control and in the autoregulation of local blood flow.

Bae, Y. M., Park, M. K., Lee, S. H., Ho, W. K. & Earm, Y. E. (1999). Contribution of Ca^{2+}-activated K^+ channels and non-selective cation channels to membrane potential of pulmonary arterial smooth muscle cells of the rabbit. *Journal of Physiology* **514**, 747–758.

Brown, J. N. & Nuttall, A. L. (1994). Autoregulation of cochlear blood flow in guinea pigs. *American Journal of Physiology* **266**, H458–467.

Casella, G. & Berger, R. L. (1990). *Statistical Inference*. Wadsworth, Belmont, CA, USA.

Chen, G. F. & Cheung, D. W. (1992). Characterization of acetylcholine-induced membrane hyperpolarization in endothelial cells. *Circulation Research* **70**, 257–263.

Coleman, H. A., Tare, M. & Parkington, H. C. (2001). K^+ currents underlying the action of endothelium-derived hyperpolarizing factor in guinea-pig, rat and human blood vessels. *Journal of Physiology* **531**, 359–373.

Dietrich, H. H. & Dacey, R. G. Jr (1994). Effects of extravascular acidification and extravascular alkalinization on constriction and depolarization in rat cerebral arterioles in vitro. *Journal of Neurosurgery* **81**, 437–442.

Doupnik, C. A., Davidson, N. & Lester, H. A. (1995). The inward rectifier potassium channel family. *Current Opinion in Neurobiology* **5**, 268–277.

Edwards, F. R. & Hirst, G. D. (1988). Inward rectification in submucosal arterioles of guinea-pig ileum. *Journal of Physiology* **404**, 437–454.

Edwards, F. R., Hirst, G. D. & Silverberg, G. D. (1988). Inward rectification in rat cerebral arterioles; involvement of potassium ions in autoregulation. *Journal of Physiology* **404**, 455–466.

Edwards, G., Dora, K. A., Gardener, M. J., Garland, C. J. & Weston, A. H. (1998). K^+ is an endothelium-derived hyperpolarizing factor in rat arteries. *Nature* **396**, 269–272.

Emerson, G. G. & Segal, S. S. (2001). Electrical activation of endothelium evokes vasodilation and hyperpolarization along hamster feed arteries. *American Journal of Physiology* **280**, H160–167.

Everitt, B. S. & Hand, D. J. (1981). *Finite Mixture Distributions*. Chapman and Hall, London.

Faraci, F. M. & Sobey, C. G. (1998). Role of potassium channels in regulation of cerebral vascular tone. *Journal of Cerebral Blood Flow and Metabolism* **18**, 1047–1063.

Feletou, M. & Vanhoutte, P. M. (1999). The alternative: EDHF. *Journal of Molecular and Cellular Cardiology* **31**, 15–22.

He, D. S., Jiang, J. X., Taffet, S. M. & Burt, J. M. (1999). Formation of heteromeric gap junction channels by connexins 40 and 43 in vascular smooth muscle cells. *Proceedings of the National Academy of Sciences of the USA* **96**, 6495–6500.

Hille, B. (1992). *Ionic Channels of Excitable Membranes*. Sinauer Associates, Sunderland, MA, USA.

Hinojosa-Laborde, C., Frohlich, B. H. & Cowley, A. W. Jr (1991). Contribution of regional vascular responses to whole body autoregulation in conscious areflexic rats. *Hypertension* **17**, 1078–1084.

Hirst, G. D. & Edwards, F. R. (1989). Sympathetic neuroeffector transmission in arteries and arterioles. *Physiological Reviews* **69**, 546–604.

Hirst, G. D. & Neild, T. O. (1978). An analysis of excitatory junctional potentials recorded from arterioles. *Journal of Physiology* **280**, 87–104.

Hirst, G. D. & van Helden, D. F. (1982). Ionic basis of the resting potential of submucosal arterioles in the ileum of the guinea-pig. *Journal of Physiology* **333**, 53–67.

Hultcrantz, E. (1988). Clinical treatment of vascular inner ear diseases. *American Journal of Otolaryngology* **9**, 317–322.

Jiang, Z. G. & North, R. A. (1991). Membrane properties and synaptic responses of rat striatal neurones in vitro. *Journal of Physiology* **443**, 533–553.

Jiang, Z. G. & Nuttall, A. L. (2000*a*). Two types of smooth muscle cells in guinea pig cochlea spiral modiolar artery. *FASEB Journal Abstracts* **14** (addendum), LB9.

Jiang, Z. G. & Nuttall, A. L. (2000*b*). Two functional states of the smooth muscle cells in cochlea spiral modiolar artery of guinea pigs. *Association for Research in Otolaryngology Midwinter Research Meeting Abstract* **23**, 202.

Jiang, Z. G., Qiu, J.-H., Ren, T.-Y. & Nuttall, A. L. (1999). Membrane properties and the excitatory junction potentials in smooth muscle cells of cochlea spiral modiolar artery in guinea pigs. *Hearing Research* **138**, 171–180.

Jiang, Z. G., Si, J. Q. & Nuttall, A. L. (2001). Acetylcholine induces hyperpolarization by opening calcium-activated K^+ channels via a NO-independent mechanism in guinea pig spiral modiolar artery. *Association for Research in Otolaryngology Midwinter Research Meeting Abstract* **24**, 29–30.

Kimura, R. S. (1986). Animal models of inner ear vascular disturbances. *American Journal of Otolaryngology* **7**, 130–139.

Klieber, H. G. & Daut, J. (1994). A glibenclamide sensitive potassium conductance in terminal arterioles isolated from guinea pig heart. *Cardiovascular Research* **28**, 823–830.

Knot, H. J. & Nelson, M. T. (1995). Regulation of membrane potential and diameter by voltage-dependent K^+ channels in rabbit myogenic cerebral arteries. *American Journal of Physiology* **269**, H348–355.

Knot, H. J. & Nelson, M. T. (1998). Regulation of arterial diameter and wall [Ca^{2+}] in cerebral arteries of rat by membrane potential and intravascular pressure. *Journal of Physiology* **508**, 199–209.

Knot, H. J., Zimmermann, P. A. & Nelson, M. T. (1996). Extracellular K^+-induced hyperpolarizations and dilatations of rat coronary and cerebral arteries involve inward rectifier K^+ channels. *Journal of Physiology* **492**, 419–430.

Nelson, M. T., Patlak, J. B., Worley, J. F. & Standen, N. B. (1990). Calcium channels, potassium channels, and voltage dependence of arterial smooth muscle tone. *American Journal of Physiology* **259**, C3–18.

Osol, G. & Halpern, W. (1985). Myogenic properties of cerebral blood vessels from normotensive and hypertensive rats. *American Journal of Physiology* **249**, H914–921.

Prior, H. M., Yates, M. S. & Beech, D. J. (1998). Functions of large conductance Ca^{2+}-activated (BK_{Ca}), delayed rectifier (K_V) and background K^+ channels in the control of membrane potential in rabbit renal arcuate artery. *Journal of Physiology* **511**, 159–169.

Quayle, J. M., Dart, C. & Standen, N. B. (1996). The properties and distribution of inward rectifier potassium currents in pig coronary arterial smooth muscle. *Journal of Physiology* **494**, 715–726.

Quayle, J. M., McCarron, J. G., Brayden, J. E. & Nelson, M. T. (1993). Inward rectifier K^+ currents in smooth muscle cells from rat resistance-sized cerebral arteries. *American Journal of Physiology* **265**, C1363–1370.

Quayle, J. M., Nelson, M. T. & Standen, N. B. (1997). ATP-sensitive and inwardly rectifying potassium channels in smooth muscle. *Physiological Reviews* **77**, 1165–1232.

Sandow, S. L. & Hill, C. E. (2000). Incidence of myoendothelial gap junctions in the proximal and distal mesenteric arteries of the rat is suggestive of a role in endothelium-derived hyperpolarizing factor-mediated responses. *Circulation Research* **86**, 341–346.

Schubert, R., Serebryakov, V. N., Engel, H. & Hopp, H. H. (1996). Iloprost activates K_{Ca} channels of vascular smooth muscle cells: role of cAMP-dependent protein kinase. *American Journal of Physiology* **271**, C1203–1211.

Schuknecht, H. F. & Gacek, M. R. (1993). Cochlear pathology in presbycusis. *Annals of Otology, Rhinology and Laryngology* **102**, 1–16.

Setoguchi, M., Ohya, Y., Abe, I. & Fujishima, M. (1997). Stretch-activated whole-cell currents in smooth muscle cells from mesenteric resistance artery of guinea-pig. *Journal of Physiology* **501**, 343–353.

Si, J. Q., Jiang, Z. G. & Nuttall, A. L. (2001). Nitric oxide activates ATP-sensitive K^+ channels of the smooth muscle cells in cochlear spiral modiolar artery of guinea pigs. *Association for Research in Otolaryngology Midwinter Research Meeting Abstract* **24**, 29.

Suvatne, J., Barakat, A. I. & O'Donnell, M. E. (2001). Flow-induced expression of endothelial Na-K-Cl cotransport: dependence on K^+ and Cl^- channels. *American Journal of Physiology – Cell Physiology* **280**, C216–227.

Suzuki, T., Ren, T., Nuttall, A. L. & Miller, J. M. (1998). Age-related changes in cochlear blood flow response to occlusion of anterior inferior cerebellar artery in mice. *Annals of Otology, Rhinology and Laryngology* **107**, 648–653.

Tani, H., Saito, D., Kusachi, S., Nakatsu, T., Hina, K., Ueeda, M., Watanabe, H., Haraoka, S. & Tsuji, T. (1990). Autoregulation by the right coronary artery in dogs with open chests; comparison with the left coronary artery. *Pflügers Archiv* **416**, 442–447.

Weidelt, T., Boldt, W. & Markwardt, F. (1997). Acetylcholine-induced K^+ currents in smooth muscle cells of intact rat small arteries. *Journal of Physiology* **500**, 617–630.

Wellman, G. C., Quayle, J. M. & Standen, N. B. (1998). ATP-sensitive K^+ channel activation by calcitonin gene-related peptide and protein kinase A in pig coronary arterial smooth muscle. *Journal of Physiology* **507**, 117–129.

Welsh, D. G. & Segal, S. S. (1998). Endothelial and smooth muscle cell conduction in arterioles controlling blood flow. *American Journal of Physiology* **274**, H178–186.

Yamamoto, Y., Fukuta, H., Nakahira, Y. & Suzuki, H. (1998). Blockade by 18β-glycyrrhetinic acid of intercellular electrical coupling in guinea-pig arterioles. *Journal of Physiology* **511**, 501–508.

Zhang, H., Inazu, M., Weir, B. & Daniel, E. (1994). Endothelin-1 inhibits inward rectifier potassium channels and activates nonspecific cation channels in cultured endothelial cells. *Pharmacology* **49**, 11–22.

Acknowledgements

The authors thank Ms Yuqin Yang for her excellent technical support, and Dr Dennis Trune and Dr Tianying Ren for reading of the manuscript. The work was supported by grants from the Deafness Research Foundation (Z.G.J.), Oregon Medical Research Foundation (Z.G.J.) and NIH NIDCD DC00105 (A.L.N.).

Corresponding author

Z.-G. Jiang: Oregon Hearing Research Center, NRC04, Oregon Health and Science University, Portland, OR 97201, USA.

Email: jiangz@ohsu.edu